Development of a High Repetition X-ray Pinhole Camera

Contact *scott.harrison.1@mac.com*

S.G.S. Harrison, R. Heathcote, R.J. Clarke, J.S. Green, M. Notley, and D.C. Carroll
Central Laser Facility, STFC
Rutherford Appleton Laboratory, Didcot, UK

D. Neely
SUPA, University of Strathclyde
Glasgow, UK

Introduction

In plasma interactions, the greatest bremsstrahlung power is emitted around the photonic energy (where h is the Planck constant, and v is the frequency of the electromagnetic waves) equal to the electron temperature (T_e). For hot plasmas, where $hv \sim T_e$, the radiation falls in the spectral range of soft x-rays (~8 keV). Imaging the x-ray radiation is sufficient, in theory, to measure the spatial profile of the interaction region; that will enable identification of any unusual features or abnormalities to the spatial profile of the plasma to be analysed and diagnosed.

The development of a high repetition, no film imaging system would be a welcome addition to the diagnostics available in the Vulcan laser target areas. It would allow multiple x-ray images to be taken without the need to gain access to the interaction chamber, increasing the shot rate.

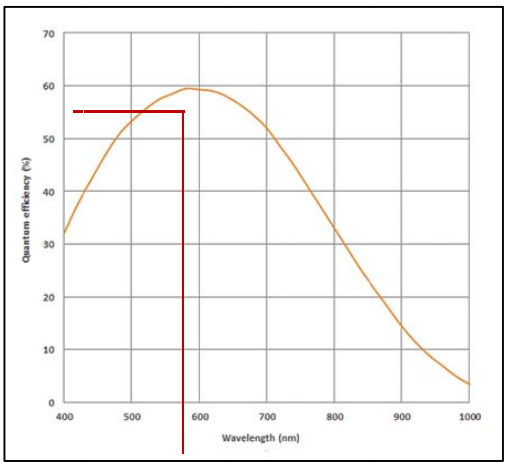

Figure 1. The quantum efficiency of the Andor Neo sCMOS. The red line corresponds to the peak output of the P43 phosphor plate[1].

When using x-rays to image, a lens cannot be used to focus the image onto the detector, as no appropriate lens materials are available. Instead, a pinhole camera can be utilised. The advantages of a pinhole camera are: a wide angular field, an almost infinite depth of focus, and are free from linear distortion. The drawbacks of a pinhole camera are; they have comparatively poor imaging resolution (when compared to systems with lenses), and produce dim images (with respect to systems with lenses).

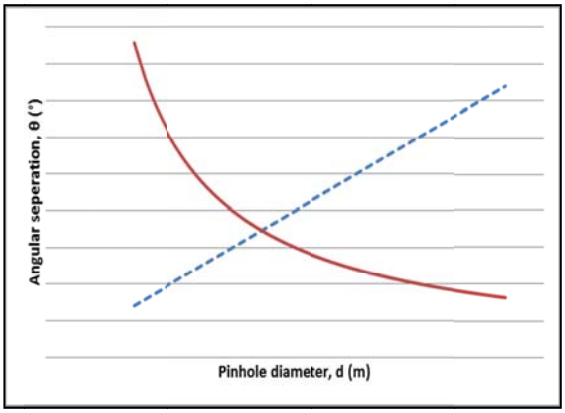

Figure 2. Sketch of the angular resolution in a pinhole camera as a function of pinhole diameter in the geometric limit (dashed line) and the diffraction limit (solid line). Where they cross indicates the optimum pinhole diameter.

To enable a diagnostic to run at a high repetition rate it is ideal that we move away from film based detectors and use digital detectors such as CCD cameras. This means the data is immediately digitised and time and effort is saved that would otherwise be used on changing over film packs. To use digital based detectors such as CCD cameras on experiments with high energy ultrahigh intensity interactions, such as with the Vulcan laser, they need to be placed outside the interaction chamber and be shielded. This is due to large electromagnetic pulses (EMP) and current beams that are generated in the interaction which induce surges of current in the electronics which cause them to malfunction and become damaged.

The image plane of the pinhole should ideally be within the target interaction chamber otherwise the pinhole camera becomes unwieldy in size and is restricted to locations where ports are located. This means that the x-ray image formed at the image plane needs to be relayed outside the chamber to where the digital detector, such as a CCD camera, is located such that it won't suffer from induced current surges.

To get the image from the pinhole camera to the CCD camera, the image must be relayed to a suitable port in the interaction chamber. A fibre optic bundle can be used

for this purpose, as it is flexible, and doesn't allow any interference to distort the signal it carries. But the fibre optic bundle and the CCD camera that are to be used are not suited to x-ray radiation (see figure 1), a phosphor must be used to luminesce the visible range of the electromagnetic spectrum when x-rays are incident upon it. The P43 phosphor screen was chosen for its strong emission in the visible spectrum (peak wavelength at 540 nm) and for its short decay time (1ms)[1].

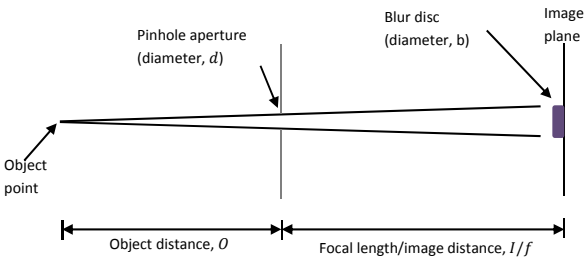

Figure 3. A ray diagram showing the x-ray path and defining measurements within the pinhole camera.

Theory

There are a few points to be considered before undertaking the development of this diagnostic array with regards to fibre optical coupling to CCD. We have to consider the limitations on the resolution of the system, and the CCD detector's dynamic range must be taken into account. Finally, the basic pinhole resolution limit needs to be taken into account, as each component in the setup will have a differing resolution.

In a pinhole camera, virtually all points are in the same focus, determined by the size of the aperture. If the aperture is too small, the point spread function will cause the image to become blurry due to diffraction events. And if the aperture is too large, geometric blurring increases. This gives the pinhole camera two resolution limits; shown in Figure 2. One defined by the Airy diffraction limit, that is embodied in the Rayleigh criterion ($\Delta\theta = \frac{1.22\lambda}{d}$), where λ is the wavelength of the photons and d is the aperture diameter. The other is the basic geometry of the image blur at the end of the pinhole camera, which is calculated as the ratio of the pinhole diameter to the camera length ($\Delta\vartheta = \frac{d}{L}$). L is the distance from the object to the image.

The geometric blur (b_G) is dependent upon the aperture diameter (d), image distance (I), and the object distance (O); shown in equation 1.

$$b_G = d\left(\frac{I+O}{O}\right) = d(1+M) \qquad \text{(Equation 1)}$$

Where $M$is the magnification of the pinhole camera; defined as the image distance divided by the object distance (shown in Figure 3).

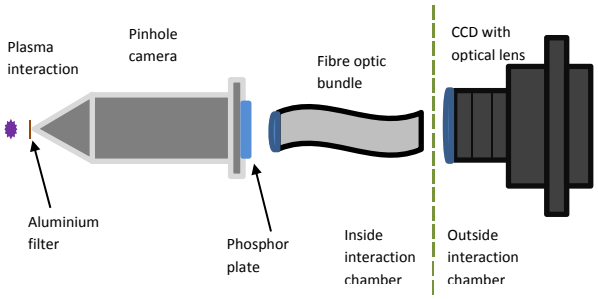

Figure 4. A schematic diagram illustrating the diagnostic setup. The dotted green line represents a window leading out of the interaction chamber.

As light passes through the aperture it diffracts, which spreads the image onto the screen and can create a Fraunhofer diffraction pattern. As the pinhole diameter decreases, the effects of diffraction are more noticeable (it is an angular effect, so is proportional to the focal length too):

$$b_D = 2.44\lambda f\left(\frac{1}{d}\right) \qquad \text{(Equation 2)}$$

The focal length of the pinhole camera is the distance from the pinhole to the image plane. By combining these two limits, one can determine the optimum pinhole diameter for wavelength and magnification specific scenarios:

$$d = \sqrt{\frac{2.44\lambda f}{(1+M)}} \qquad \text{(Equation 3)}$$

Using equation 3, we can optimise the pinhole diameter for a specific energy of x-rays. For example, for 8keV x-rays, the ideal pinhole diameter is 3.7µm.

The resolution of the x-ray imaging diagnostic is only as good as the weakest part of the chain. There are three additional points to the pinhole itself in the setup which come under scrutiny; the phosphor plate, the fibre optic bundle, and the CCD camera. The phosphor plate's resolution is inversely proportional to the thickness of the phosphor layer. The resolution is approximated as: $R_L = \frac{500}{D}$, where $D$is the thickness of the phosphor layer in µm, and the resolution is calculated in linepairs per millimetre (lp/mm). Using a white light interferometry probe scan, the thickness of the phosphor layer was calculated as 27 ± 3 µm, giving a resolution of 18.5 lp/mm. The next element in the diagnostic array is the fibre optic bundle. The bundle is made up of many multifibres, each 50 µm by 50 µm, that contain 25 fibre optic fibres each. The shortest distance between the centre of two adjacent fibres is 10 µm, which gives the bundle a resolution of 50 lp/mm. The defining resolution factor of the CCD is the size of the pixels onto which the plasma image is focussed onto. The pixels are 6.5 µm x 6.5 µm, giving the CCD a spatial resolution of 76.8 lp/mm. These results determine that the effective

resolution of the system is defined by the resolution of the phosphor plate and it is limited to 18.5 lp/mm.

With all the theory considered, the diagnostic components can be setup for the test period, to determine the effectiveness of this conception.

The pinhole camera and fibre optic bundle remain inside the interaction chamber (as shown in Figure 4), as they have no electronic components; and are therefore unaffected by transient disturbances. Additional lead shielding is needed to attenuate high energy x-rays and gamma rays, which have not passed through the pinhole, from reaching the phosphor plate and adding unwanted noise. Between the plasma interaction and the pinhole camera an aluminium filter is used to block out all visible light coming from the interaction. Beyond a window on the interaction chamber, the CCD camera and diagnostic PC will record the spatial profile of the plasma. The CCD camera is out of direct line of sight of the interaction.

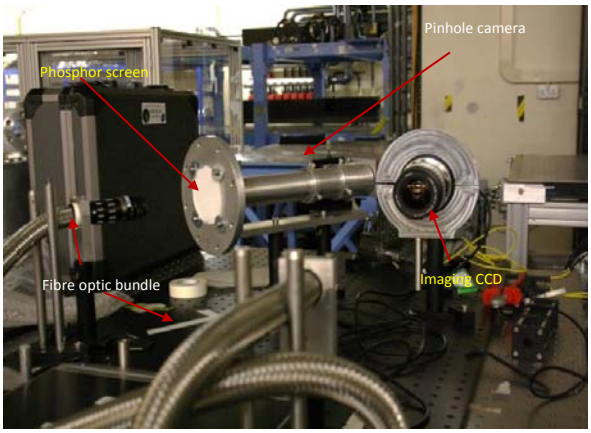

Figure 5. Photograph of the diagnostic setup showing the phosphor plate, the pinhole camera, the fibre optic bundle, and the imaging CCD.

Inside the interaction chamber, the pinhole camera is positioned approximately 40mm from the target. This will produce an image at the phosphor plate that has been magnified ten times. The fibre-optic bundle has a lens at the front end which is focussed onto the back of the phosphor plate. An image forms at the other end of the bundle, which is seen from outside the chamber by the Andor Neo sCMOS camera.

Test Results

The diagnostic array was tested during the TAW access period of March 2014. During this time, the pinhole camera imaged several shots with a selection of different combinations of filters and pinhole diameters. The Andor CCD was triggered 20 ms before each shot, and the rolling shutter was open for half a second to guarantee the chip was subject to significant numbers of photons.

Before inserting a pinhole into the nose of the camera, we tested the imaging system without using any pinholes or filters, this is to test if the phosphor lights up and that emission is imaged successfully to the camera The nose of the pinhole camera gave an effective pinhole diameter of 2 mm. Figure 5 shows the image recorded on the Andor Neo. The image is extremely blurred, which is to be expected with such a large pinhole diameter due to geometric blurring (equation 1).

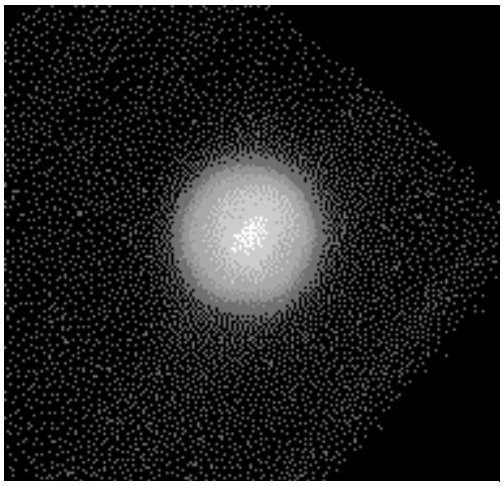

Figure 5. Image is formed on the phosphor plate. Andor Solis recorded ~15000 counts per pixel in the image.[No filters, and 2mm pinhole]. The image has been cropped and enlarged.

Next, we included a 300 um pinhole and also a 16 um aluminium filter to remove any signal from the visible range of the electromagnetic spectrum. This was a key stage in the testing process as it would allow us to see whether the image seen in figure 5 is a result of the phosphor plate luminescing due to x-ray radiation, or whether it is visible light leaking through the phosphor plate. Looking at figure 6, one can clearly see an image, comparable to that from figure 5, formed on the phosphor plate. The image is duller than in figure 5, with a count rate of around 1500 per pixel in the centre of the image. This is to be expected as fewer photons can pass through the pinhole as its diameter decreases. However promising the results were, there was a compromise to the quality of data brought about due to the streaks across each fibre optic image. We believe that these streaks are generated in the fibre optic bundle and are a signature of the bundle used. They are not present in figure 5; this is most likely due to the higher pixel count. Another explanation for this recurring phenomenon is that light from the interaction is scattering off of windows then onto the bundle and into the camera. The lower count in figure 6 means the noise and interference comes out of the background further than it does in the test image (figure 5). The fainter, larger circle on the fibre bundle, that is visible in figure 6, is the phosphor plate.

Conclusion and Future Work

Overall, the test period provided some positive initial results, including a proof of principle for this imaging diagnostic, which shows it be potentially useful in future applications. Going to a smaller pinhole is required to ensure the images are in focus and that the diagnostic is useful. However in doing this the number of x-rays reaching the phosphor will decrease, making the image dimmer. Therefore one of the changes to make upon further use of the diagnostic is to change the CCD used so that the signal may be amplified to compensate for the lower count per pixel ratio. The focus of future work should be to diagnose and remove the cause of the interference, shown clearly in figure 6 that is expected to come from the fibre bundle. For the next stage of testing an alternate fibre optic bundle should be utilised to properly diagnose whether it was a problem with that specific bundle. Another thing to note is that the phosphor plate is sensitive to electrons and has a high photon to electron conversion rate. This means that when the pinhole camera is used it will require a magnet to deflect the electrons and prevent them from reaching the phosphor plate.

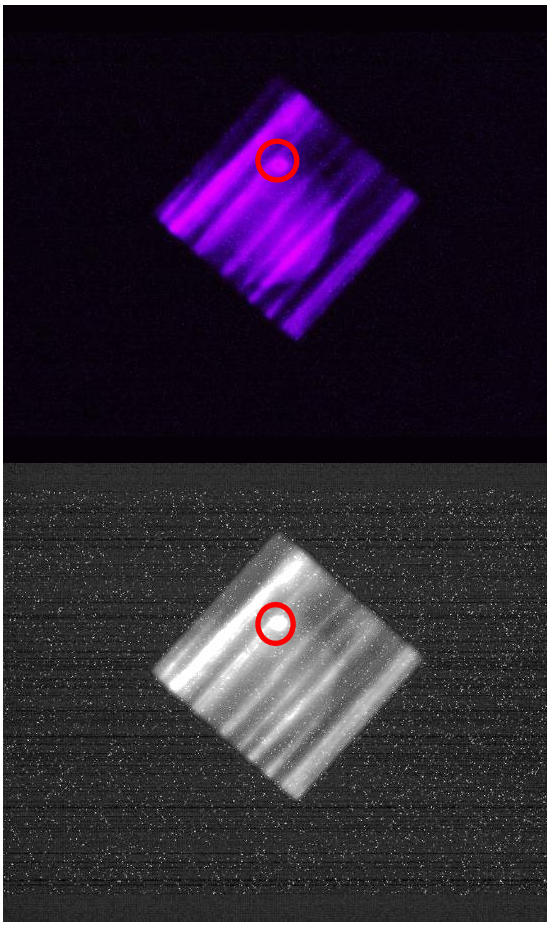

Figure 6. Signal recorded on Andor neo was comparable to the no pinhole image as we see an image of the plasma formed. Approximately 1500 counts per pixel for the image of the plasma (shown in the red circle) for two separate shots.

References

[1] PROXI VISION. *Phosphor Screens.* [Online]. Available from: http://www.proxivision.de/datasheets/Phosphor-Screen-PR-0056E-03.pdf. [Accesed: 12th December 2013]

[2] ANDOR. (2012) *Neo 5.5 sCMOS.* [Online] Available from: http://www.andor.com/scientific-cameras/neo-and-zyla-scmos-cameras/neo-55-scmos. [Accessed: 21st May 2014]